Prediction of Positive Refractivity Gradients for Line-of-Sight Microwave Radio Paths

By J. A. SCHIAVONE

Estimating obstruction fading on line-of-sight microwave radio paths requires statistics on positive refractivity gradients in the lowest 100 meters of the atmosphere. In this paper, we describe a semiempirical climatological model that predicts quantitatively the occurrence frequency of positive refractivity gradients and the geographical variation of this frequency within the contiguous United States. The occurrence frequency is parameterized by six factors, for which numerical values are obtained from available climatological and physiographical data. By modeling the two diurnal atmospheric boundary layer regimes with separate probability density functions, we produce cumulative probability distributions for refractivity gradients. The model is normalized using measured refractivity gradient distributions available for 17 sites within the United States. The model can be used for line-of-sight microwave radio path engineering; a companion paper presents a method for determining antenna heights.

I. INTRODUCTION

Line-of-sight microwave radio transmission performance is susceptible to atmospheric conditions, in particular to spatial variations in the microwave refractive index. Nearly always during the day and frequently at night, sufficient vertical mixing occurs of the low-level air layers, through which the microwave beam propagates, so that vertical refractive index gradients encountered are small. However, horizontal layers containing strong vertical gradients in air temperature and water vapor pressure, which determine the refractive index, sometimes develop at night. The presence of these layers can cause the received signal to fade (decrease in strength).

This paper addresses the meteorology of obstruction fading, which

is caused by a large positive gradient in the refractive index, which is, in turn, caused by a large positive water vapor pressure gradient. The ray path between the transmitting and the receiving antennas is lower than normal in the presence of a positive refractive index gradient, and the terrain can block the ray path when the positive gradient is sufficiently large. Although infrequent, the consequences of obstruction fading are severe: transmitted signal is steadily blocked for as long as an hour at a time. Obstruction fading can be avoided by locating microwave antennas sufficiently high above the ground.

Prolonged fades can also be caused by strong negative gradients that refract the transmitted microwave beam downward to such an extent that it ceases to illuminate the receiving antenna. Climatic conditions and path geometries in the United States are such that this is usually a secondary phenomenon compared to obstruction fading.

The presence of negative gradients of more modest proportions is associated with multiple propagation paths through the atmosphere, which cause phase interference fading (multipath fading). Phase interference fading is a major factor in microwave system design. The meteorology of multipath fading is a separate topic, and is not addressed in this paper.

Probability distributions for the occurrence of refractive index gradients have been compiled by Samson,[1] Bean et al.,[2] and Dougherty[3] from measurements of vertical profiles of meteorological parameters. The distributions are intended for use in engineering microwave paths. However, these sets of compilations are for isolated locations, and they have not been generalized to account for the varied climates to which different microwave routes are exposed.

The purpose of the present work is to devise a climatological model to predict quantitatively the geographical variation of the occurrence frequency of positive refractive index gradients within the contiguous United States. The results can be used to estimate obstruction fading occurrence on microwave radio paths to help determine optimum microwave antenna heights. The result of the model is a predicted cumulative probability distribution for positive refractive index gradients calculated for an arbitrary location within the contiguous United States for arbitrarily large gradients. The present model represents the first attempt to predict refractivity gradient probability distributions from climatological data. Ikegami et al.[4] and Akiyama and Sasaki[5] have performed fits to measured refractive index gradient distributions but without meteorological parameterization.

This model is designed to provide predictions for the 48 contiguous United States. Two submodels must be used to account for the varied climates experienced by this large geographical entity: a coastal region submodel and an interior region submodel. The interior region sub-

model is based on a relatively small experimental data base and the reliability of the overall model for interior regions is possibly lower than for coastal regions. However, since obstruction fading occurs mostly in coastal regions, the model is most reliable where it is most useful.

The predictions of this model are compared to measured distributions[1] and, in general, show good agreement. We attribute the imperfect agreement that exists in a few cases to local effects that cannot be accounted for without introducing additional complexity with the attendant risk of making the model unwieldly to implement. That is, we use a geographical resolution for the model, which has been judged optimum by weighing resolution improvements against simplicity of model use.

II. MODEL FORMULATION

The model is formulated in two stages. First, we choose parameters (Section 2.1) based on meteorological principles, to relate the occurrence frequency and magnitude of refractive index gradients to available climatological and physiographical data. Second, we develop a method for producing a refractive index gradient probability distribution from these parameters (Section 2.2). The model is quantified by comparison with measured distributions.[1] We make final minor adjustments to the model to provide consistency with information on the geographical distribution of obstruction fading gleaned from transmission performance experience in the Bell System.[6]

2.1 Meteorology

The refractive index, n, for microwaves can be expressed as refractivity,[7]

$$N = 10^6(n - 1) = \frac{77.6}{T}\left(P + 4810\,\frac{e}{T}\right), \qquad (1)$$

where N is the refractivity in N-units, T is the air temperature in kelvin, P is the air pressure in millibars, and e is the water vapor pressure in millibars. Water vapor pressure is the governing contributor to producing positive refractivity gradients (N') at night. Therefore, a positive refractivity gradient model must predict climatologically the frequency of occurrence of positive e gradients.

During obstruction fading, the important part of the microwave beam generally lies within the lowest 100 m of the atmosphere and available radio meteorological data have been obtained, therefore, for 100 m. However, since probability distributions are functions of height increments, we present a method (Section 2.2) for using a height increment appropriate to the particular application.

Several mechanisms can produce inverted (positive gradient) water vapor vertical profiles:

(*i*) Condensation of water vapor at the bottom of a surface-based nocturnal temperature inversion, e.g., dew or ground fog, causes absolute humidity to decrease there.[8] However, the amount of water vapor condensed is insufficient to produce large gradients across a layer as thick as 100 m.

(*ii*) Strong convection processes in relatively dry air can produce water vapor inversions within the daytime boundary layer.[9] Development of a nocturnal temperature inversion could cause the water vapor inversion to persist throughout some of the night. The magnitude of these gradients is insufficient to cause obstruction fading, however.

(*iii*) Uplands generally receive more rainfall than surrounding lowlands, provided the altitude difference is large enough. When situated within relatively dry lowland regions, daytime evaporation from the uplands can produce elevated moist air layers. Such an effect has been observed.[10] Nocturnal radiative temperature inversions could cause the water vapor inversion to persist during the night. Such a mechanism is greatly limited geographically, however.

(*iv*) Nocturnal advection of moist air can produce inverted water vapor profiles. Nocturnal land breezes at water body-land interfaces, are a possible mechanism. However, the effects of land breezes usually do not penetrate more than a few tens of kilometers inland and, thus, cannot explain severe obstruction fading observed farther inland.

(*v*) We propose large-scale advection of moist air as the mechanism for producing most of the obstruction fading on line-of-sight microwave radio routes. This mechanism is supported by various characteristics of the limited information on observed obstruction fading in the Bell System:[6] (1) Often large areas are affected by a single episode. (2) The length of microwave paths requires vertical gradients to be horizontally homogeneous over approximately 40-km distances to produce fading. (3) Relatively flat areas are especially susceptible; flat areas are conducive to large-scale, low-level advection at night. (4) Regions within 300 km of coastlines are especially susceptible; 300 km is the distance air could travel at typical speeds at approximately 100-m altitude during 12 night hours. (5) Finally, a study of a severe fading episode in the Bell System showed that the onset of obstruction fading occurred later for greater distances from the coast.

An understanding of the details of the proposed large-scale moisture advection mechanism requires knowledge of atmospheric motion on various distance scales. We will now discuss atmospheric motion within the boundary layer, across the continent, and within air masses.

Obstruction fading usually occurs during fine weather conditions, when anticyclonic air masses envelop the affected region. Thus, the

characteristics of the boundary layer and their diurnal variation only in fine weather conditions need be considered.

During the day, solar radiation causes convective mixing which produces a relatively deep ($\gtrsim 1$ km) boundary layer which is vertically well mixed throughout. Thus, vertical gradients of water vapor and horizontal momentum are relatively small across the lowest 200 m where the microwave beam lies. Small vertical gradients of horizontal momentum produces small wind speed and direction gradients (Fig. 1a).

At night, radiative cooling of the earth's surface produces a relatively thin (as thin as $\sim$100 m) density-stable boundary layer. The high stability suppresses turbulence and very little vertical mixing occurs; water vapor inversions would be maintained once produced. Relatively large wind speed and direction gradients could be maintained across the boundary layer[11] (Fig. 1b) because of the limited vertical mixing of horizontal momentum. Calm winds often occur at the surface.

Large-scale air motion is determined by the midtropospheric ($\sim$6 km) winds. These currents steer air masses across the North American continent, in general, from west to east. Air masses that affect the
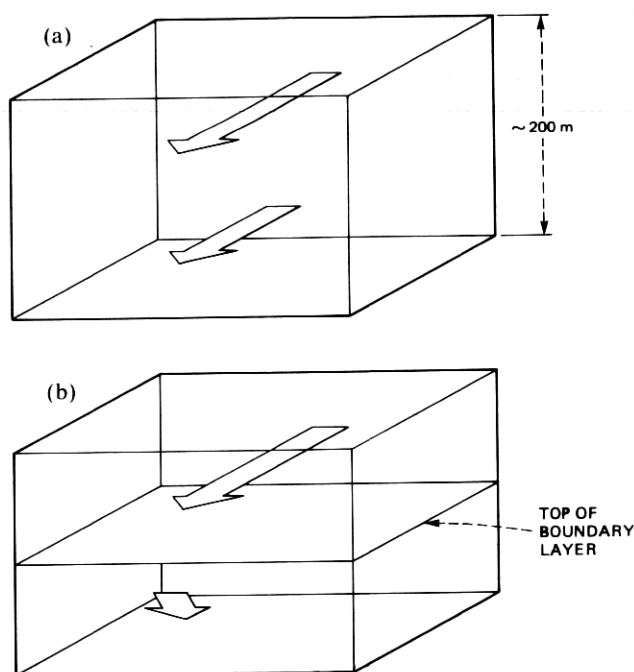

Fig. 1—Air flow in lowest 200 m. Arrows indicate relative wind speed and directions at two heights, illustrating the enhancement of differential flow at night which contributes to moisture inversions in coastal regions.

United States usually originate over northwest Canada or the eastern Pacific Ocean.[12] Pacific air masses crossing the continental divide lose much of their moisture through lifting-induced precipitation over the western mountains. Therefore, except for the west coast, air masses are relatively dry until they reach the Great Lakes, Atlantic Ocean, or Gulf of Mexico. Once they reach these large water bodies, evaporation increases their moisture content.

Air flow at moderately low levels ($\lesssim 2$ km) within anticyclonic air masses is essentially circular (for the purpose of this discussion) with respect to the air mass core, and in a clockwise direction. Thus, moderately low level winds at a given location change direction as an air mass traverses the region. Furthermore, winds near the center of the air mass are very light because of small horizontal pressure gradients; therefore, highly stratified air layers can readily form there.

The mechanism for producing water vapor inversions by the large-scale moisture advection that we are proposing is as follows: dry air masses approach the east (south) coast of the United States from the west (northwest). Before the air masses reach the coasts, moderately low level ($\lesssim 2$ km) wind flow is mainly offshore in coastal regions, thus, maintaining dry air there. As the air mass core comes sufficiently close to the coast, winds to the south and west of the air mass core shift to an onshore direction, advecting moist air inland. If the offshore–onshore wind shift occurs near sunset, the characteristics of the night-time boundary layer discussed earlier, wind speed and direction differences across it, cause moist air to be advected over the top of surface-based dry air. The differential wind speed advects moist air inland faster at approximately 200 m than at the surface. The differential wind direction, which is normally a clockwise shift with height, also contributes to maintaining faster inland penetration of moist air at approximately 200 m relative to the surface.

Production of positive e gradients at a particular site requires the site to be sufficiently close to a moisture source so that moist air can reach the site during the nocturnal stratified air regime. Measured refractivity gradient distributions[1-3] show that elevated moist layers occur most frequently near large bodies of water such as oceans, gulfs, and large lakes. However, measurements show also that elevated moist layers occur at sites too far from these large water bodies to have had them for their source of moisture. Thus, mechanisms other than large-scale advection probably also contribute to positive refractivity gradients. Each mechanism cannot be modeled specifically, as for large-scale moisture advection. Therefore, a large-scale moisture-advection model is used near large water bodies (coastal regions), while a mechanism-independent model is used for other areas (interior regions).

2.1.1 Coastal region

The coastal region model is parameterized by six factors relating the occurrence of positive e gradients to parameters obtainable from seasonal climatological and physiographical maps. The factors are frequency of temperature inversion occurrence, f_i; air homogeneity, H; water body proximity, D; frequency of wind direction occurrence, f_w; air moisture capacity, V; and surface moisture availability, M. The proportionality among the six factors and their individual normalization is obtained empirically from measured N' probability distributions (Section 2.2).[1] The factors f_i and H specify the occurrence of stratified air, D and f_w specify the production of positive e gradients, and V and M specify the magnitude of the positive e gradients.

The occurrence of stratified air in the lowest 100 m coincides with the existence of temperature inversions (temperature increase with height). Hosler has compiled maps of the occurrence frequency of surface-based temperature inversions for four seasons within the United States.[13] The frequency of temperature inversion occurrence, f_i, whose units represent the fraction of total time that inversions occur for a given location and season, is employed as a factor in the coastal model.

For obstruction fading to occur, large positive e gradients must occur over the entire microwave path (a standard path length of 40 km is assumed in this work). Thus, the horizontal homogeneity of the stratified air, which is determined by the flatness of the terrain profile, must be large for the occurrence of obstruction fading. Therefore, a factor, H, is introduced that represents the horizontal homogeneity of the stratified air. Values for this factor are obtained from a map in the United States National Atlas, "Classes of Land Surfaces Forms."[14] In this map, each location is represented by three characteristics: slope, local relief, and profile type. In the present model, each characteristic is defined as a subfactor of H,

$$H = H_1 H_2 H_3. \tag{2}$$

Numerical values of H_1, H_2, and H_3 are acquired, after all other empirically determined parameters are obtained, by comparison of the model with the geographical distribution of microwave transmission performance in the Bell System.[6] Transmission performance experience is employed since it represents the only existing *path-averaged* obstruction fading information. Table I gives the values obtained for H_1, H_2, and H_3.

It is useful to compare refractivity gradient distributions which are predicted by the present model and represent path averages, with measured distributions compiled at single points. In such cases path

Table I—Air homogeneity subfactors.
Classes are obtained from Ref. 14.

Slope Class h_1	H_1	Relief Class h_2	H_2	Profile Class h_3	H_3
A	1.0	1	1.0	a	0.7
B	1.0	2	0.9	b	0.8
C	0.8	3	0.5	c	0.8
D	0.4	4	0.5	d	1.0
		5	0.5	None	1.0
		6	0.5		

averaging is removed from the predictions. This is accomplished by setting H to its maximum value, 1.0, in those instances.

For the coastal region, production of positive e gradients requires proximity to a large water body. Moist air originating at the coastline at sunset can penetrate a maximum distance inland during the nocturnal stratified air regime. Therefore, we propose the following smoothed-step distance function to represent this effect:

$$D = [1 + (d/d_0)^4]^{-1}, \tag{3}$$

where d is the minimum distance to an ocean, gulf, or one of the Great Lakes and $d_0 = 300$ km, as determined by the maximum distance inland that the air can penetrate during 12 hours when moving at an average speed at a height of approximately 100 m.

For every location there is a wind direction that maximizes the relative advection of moist air over dry air. The appropriate direction varies with distance to and shape of the coastline nearest the site. The procedure for specifying this direction for different sites is discussed in Appendix A. We propose that the production of positive e gradients is proportional to the frequency, f_w, that wind blows along this direction. Values for f_w, in units of fraction of total time, are obtained from frequency distributions of surface wind direction.

The magnitude of the e gradients formed depends upon the water vapor capacity of the air. The water vapor capacity, in turn, depends upon air temperature, T. The saturation vapor pressure function, $e_s(T)$, is a logical choice to represent the dependence of water vapor capacity on air temperature. It is proposed that a water vapor capacity factor be represented by

$$V = \frac{e_s(T)}{e_{s0}}, \tag{4a}$$

where $e_s(T)$ is in millibars and $e_{s0} = 50$ mb, an approximate upper limit for naturally occurring vapor pressures. The function $e_s(T)$ can be represented by[8]

$$e_s(T) = \exp[21.71 - 5433/T], \tag{4b}$$

where T is in kelvin. Temperatures used are those obtained from monthly average temperature maps of the United States.[16]

The magnitude of the e gradients produced by advection from large water bodies is reduced if substantial smaller local sources of water exist at the site. This is caused by surface water evaporating into the dry lowest air layer. This effect is modeled with a surface moisture factor

$$M_C = \frac{m_1}{m_0 + m},$$
(5)

where m is a surface moisture index obtained from a map of moisture regions,[17] $m_0 = 70$, and $m_1 = 20$, obtained by comparison with measured N' distributions.[1] The subscript C denotes the coastal region since a different moisture factor is employed for the interior region.

In summary, the six factors used to determine the occurrence of positive e gradients in the coastal region are f_i, H, D, f_w, V, and M_C.

2.1.2 Interior region

The model for interior sites is a modification of that developed for the coastal sites. The two factors representing the production of stratified air layers, H and f_i, are the same as for the coastal model. However, the two factors representing the production of positive e gradients, D and f_w, are combined into a single constant factor, A'. This is required because it is not feasible to take into account the variety of mechanisms thought to contribute to gradient production in interior regions. Determination of A' is discussed below. Finally, of the two factors representing the magnitude of the e gradient produced, V and M, only M need be modified. This modification is required since the surface moisture index, m, provides the necessary information regarding the availability of moisture from local sources. Thus, the proportionality between M and m is inverted with respect to the coastal site model. The interior region model for M is

$$M_I' = \frac{m + m_2}{m_3}.$$
(6a)

Since the relative advection factor, A', is constant, m_3 can be absorbed into it yielding $a = A'/m_3$. We determine empirically that $a = 4.7 \times 10^{-5}$ and $m_2 = 100$ (Appendix B). Equation (6a) can be rewritten as

$$M_I = m + m_2.$$
(6b)

The five factors used to determine the occurrence of positive e gradients in the interior region are f_i, H, a, V, and M_I.

The interior model, instead of the coastal model, is applied to the Pacific Coast of the United States. The large-scale moisture-advection

mechanism upon which the coastal model is based is not valid for the Pacific Coast since air masses which cross the coast already contain much moisture. Furthermore, relatively high coastal mountain ranges prevent low-level nocturnal differential advection.

2.2 Refractivity gradient probability distributions

Examination of measured N' cumulative probability distributions[1-3] indicates that the shape of each curve is characterized by three features when plotted on normal probability axes (Fig. 2): a central linear segment and positive and negative tails. Ikegami et al.[4] and Akiyama and Sasaki[5] have noted these features and have attempted to fit each with different mathematical formulas, but no attempt was made to interpret them meteorologically. We hypothesize that the central segment is produced by an atmospheric regime characterized by at least some vertical air mixing, and the tails are produced by a regime characterized by stratified air. In general, the tails are distributed asymmetrically about the mean. This is expected, since different meteorological mechanisms produce positive and negative gradients in stratified air. Therefore, a mixture of at least three distributions is required to represent the total cumulative probability distribution completely. In view of the complexity of handling a mixture of three distributions relative to two distributions, and since only positive N' gradients are of concern for obstruction fading, we do not attempt to model that half of the cumulative probability distribution where N' is more negative than the mean. Therefore, we employ a mixture of two distributions.
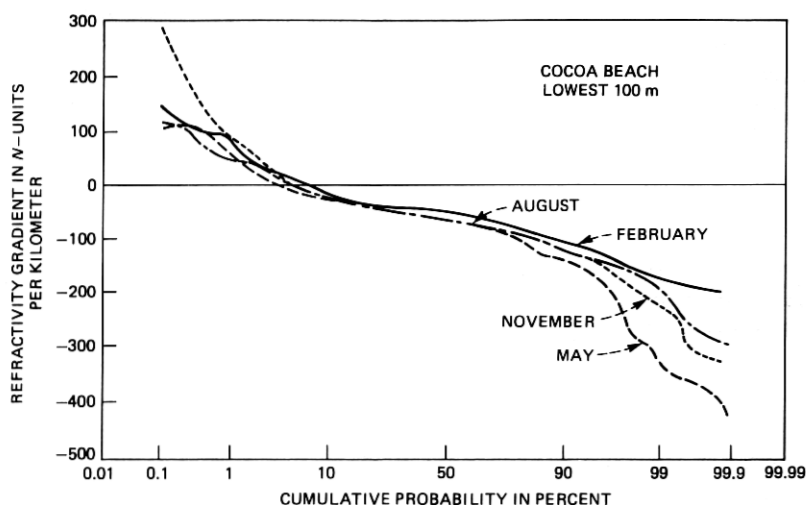

Fig. 2—One of 17 measured refractivity gradient distributions compiled by Samson.[1]

In general, the mixed regime distribution comprises approximately 80 percent of the total distribution (see discussion of p^* below). Furthermore, it is well documented that mean refractivity gradients in mixed air are similar to those expected from normal daytime vertical distributions of water vapor, temperature, and air pressure.[7,18] Therefore, since gradients developed during the stratified regime evolve from those existing during the mixed regime, and since the negative-going half of the total distribution is not modeled (relieving the need to account for asymmetry), it is reasonable to assume that each of the two component distributions can be represented by normal distributions that share the same mean, μ. Figure 3 illustrates this assumption. These component distributions are given by the probability density functions

$$p_m(N') = (2\pi\, \sigma_m^2)^{-1/2}\exp\left[-\frac{1}{2}\left(\frac{N'-\mu}{\sigma_m}\right)^2\right] \qquad (N' \geq \mu), \qquad (7a)$$

$$p_s(N') = (2\pi\, \sigma_s^2)^{-1/2}\exp\left[-\frac{1}{2}\left(\frac{N'-\mu}{\sigma_s}\right)^2\right] \qquad (N' \geq \mu), \qquad (7b)$$

where m and s denote the mixed and stratified regimes, respectively. The total probability density function is given by

$$p(N') = (1 - p^*)p_m + p^*p_s, \qquad (8)$$

where p^* is the proportion of mixture for the two component distributions.

We empirically compared a mixture of two distributions with Samson's U.S. data and determined that $p^* = 0.2$ and $\sigma_m = 15$ N-units/km and that both are essentially invariant with respect to location and season. Bean et al. have compiled seasonal maps of the average refractivity gradient in the lowest 1-km depth.[2] This data is used to specify μ as a function of location.

The standard deviation for the stratified regime, σ_s, is parameterized separately for the coastal and interior regions by

$$\sigma_{sC} = \sigma_0(f_iH)^{1/2}(Df_wVM_C)^{1/4} \qquad (9a)$$

and

$$\sigma_{sI} = \sigma_0(f_iH)^{1/2}(aVM_I)^{1/4}, \qquad (9b)$$

where σ_0 is a constant for a given layer thickness and path length, and the exponents, ½ and ¼, are determined empirically. Both σ_{sC} and σ_{sI} are calculated for each site and season, and the larger of the two is employed to calculate p_s for each season. Total probability, $p(N')$, is calculated for each season and the seasonal probabilities are averaged to produce an annual probability density function for each site. Finally,
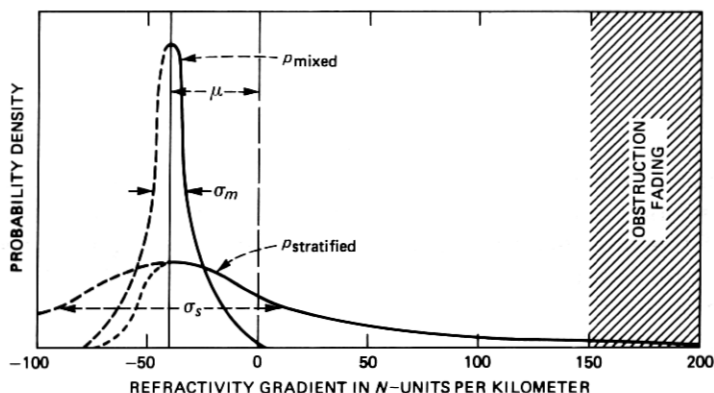
Fig. 3—Illustration of two probability density functions employed to represent a refractivity gradient distribution. Dashed portions of the functions denote halves which are not modeled. The dotted line denotes a possible "true" negative-going half of the stratified distribution which is, in general, asymmetric about the mean.

the probability density functions are integrated from $+\infty$ to μ to produce N' cumulative probability distributions for positive N'.

Samson's 17 measured N' distributions[1] were used to determine empirically that σ_0 for a 100-m-deep layer is 440 N-units/km. N' distributions have been compiled at several sites for surface layer thicknesses (Δz) different from 100 m. Samson compiled annual distributions at Cardington, England for 75-, 150-, and 500-thick layers.[1] Dougherty compiled annual distributions at Cocoa Beach, Florida for 50- and 100-m-thick layers.[3] Values for the climate parameters appropriate to each site were used in an empirical determination of σ_0 for the five available layer thicknesses. $H = 1$ was used; the reason for this choice has been discussed in Section 2.1.1.

The results are plotted against $(\Delta z)^{-1/4}$ in Fig. 4 and indicate such a relationship. The line in Fig. 4 represents $\sigma_0(\Delta z) = 1400/\Delta z^{1/4}$, where Δz is in meters and σ_0 is in N-units/km. Thus, σ_0 for an arbitrary layer thickness, can be obtained from this plot.

III. RESULTS AND DISCUSSION

Complete specification of a predicted N' probability distribution is made by the parameters p^*, μ, σ_m, and σ_s. The parameters p^* and σ_m are constants; however, μ and σ_s must be specified for each season as a function of location. Bean et al. provide seasonal maps for μ measurements,[2] and Table II summarizes specification of σ_s.

It is useful to compare a few predicted distributions with measured ones to check the performance of the model. Figures 5 through 7 show examples of N' cumulative probability distributions predicted by the model for 100-m layers (thicknesses for which measured distributions
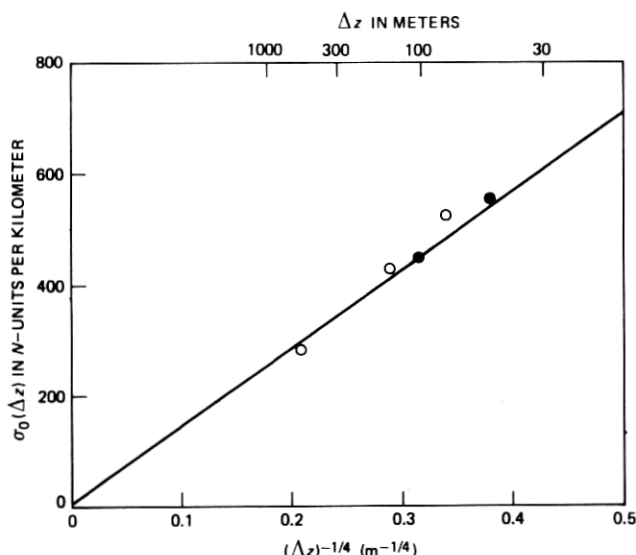
Fig. 4—Dependence of σ_0 upon surface layer thickness, Δz. Data points are derived from Samson's compilations[1] for Cocoa Beach, Florida (●), and Cardington, England (○).

are available); measured curves are also shown. Predicted curves were calculated using $H = 1$ (see Section 2.1.1). The ability of the model to successfully predict large differences in distribution shapes for two sites separated by only 500 km is illustrated by comparing the Cocoa Beach and Key West curves. The model's ability to respond to seasonal variations in both coastal and interior regions is illustrated for Cocoa Beach and Denver.

The agreement between predictions and measurements is generally good; however, it is not perfect. Each measured distribution, with a few exceptions, was compiled from approximately 900 measurements (Table III). Thus, the data point density on the distribution tails is

Table II—Summary of method for evaluating σ_s parameters.

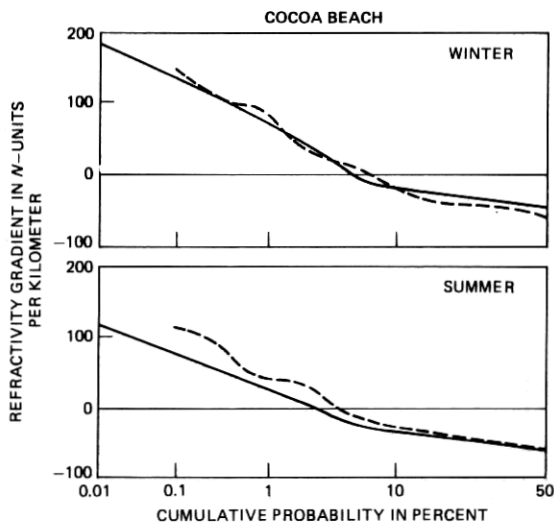| Parameter for σ_s Calculation	Equation used for Parameter Calculation	Equation Constants	Climatological Variables	Sources of Climatological Variables
f_i	—	—	f_i	Ref. 13
H	(2)	Table I	$h_1,\ h_2, h_3$	Ref. 14
D	(3)	$d_o = 300$ km	d	U.S. map
f_w	—	—	f_w	Ref. 15
V	(4)	$e_{so} = 50$ mb	T	Ref. 16
M_C	(5)	$m_o = 70, m_1 = 20$	m	Ref. 17
a	—	$a = 4.7 \times 10^{-5}$	—	—
M_I	(6b)	$m_2 = 100$	m	Ref. 17

Fig. 5—Comparison of positive refractivity gradient distributions predicted in this work (solid line) with those compiled by Samson[1] from measurements (dashed line) for a 100-m-deep layer for coastal site Cocoa Beach.

low. Therefore, some contribution to the disagreement is expected from statistical noise.

A more complete assessment of the agreement between predictions and measurements has been made by plotting predicted vs measured
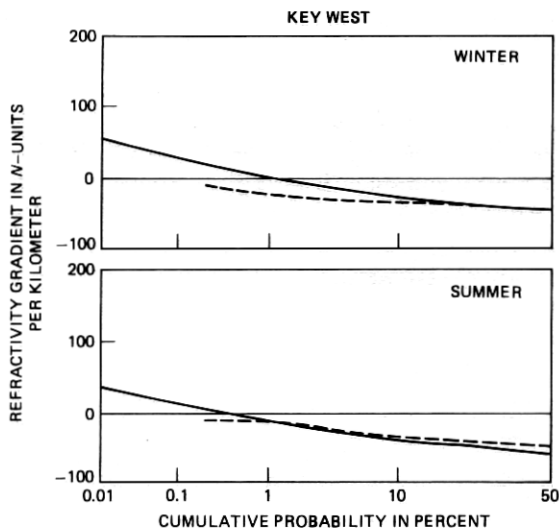

Fig. 6—Comparison of positive refractivity gradient distributions predicted in this work (solid line) with those compiled by Samson[1] from measurements (dashed line) for a 100-m-deep layer for coastal site Key West.
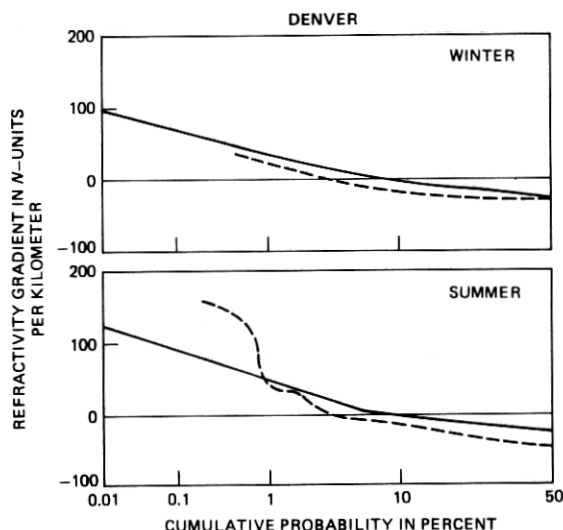
Fig. 7—Comparison of positive refractivity gradient distributions predicted in this work (solid line) with those compiled by Samson[1] from measurements (dashed line) for a 100-m-deep layer for Denver (an interior site).

annual probability for $N' \geq 100$ N-units/km for Samson's 17 sites (Fig. 8).[1] Such an evaluation requires that path averaging be removed from the predictions for comparison with point measurements. This is accomplished by setting the air horizontal homogeneity factor, H, to its maximum value (1.0) for all sites. Therefore, probabilities calculated in this manner are characteristic of a single point along the 40-km path length.

It is most useful to compare predicted and measured distributions for the largest refractivity gradients for which measured probabilities could be obtained from Samson's data.[1] As the optimum gradient for comparison, 100 N-units/km was selected. However, not all of the measured distributions for each season at a given site intersected 100 N-units/km. Therefore, for those that did not, distribution tails were extrapolated linearly on the original graphs to estimate probabilities at 100 N-units/km for those seasons. Annual values of $P(N' \geq 100$ N-units/km) were obtained by averaging the four seasonal probabilities.

Poorer agreement between predicted and measured distributions is expected for interior sites, since a single specific mechanism has not been modeled as for the coastal sites. However, obstruction fading is not a serious problem in interior regions. For all sites except four, the prediction is near the measurement. Two of the four sites are interior ones, discrepancies for which were anticipated. The four anomalous sites (Denver, El Paso, New York, and Long Beach) all show considerably higher occurrence frequency of positive gradients than pre-

Table III—Sites for which Samson's measured refractivity gradient cumulative probability distributions[1] were employed and approximate number of individual observations associated with each. Symbols in last column identify points in Figure 6.

Site	Number of Observations	Symbol	Site	Number of Observations	Symbol
Atlanta, GA	880	A	Long Beach, CA	880	J
Brownsville, TX	880	B	Miami, FL	880	K
Charleston, SC	880	C	New York, NY	880	L
Cocoa Beach, FL	1280	D	Oakland, CA	850	M
Columbia, MO	880	E	San Diego, CA	880	N
Denver, CO	880	F	Seattle, WA	880	O
El Paso, TX	1280	G	Tatoosh Island, WA	880	P
Joliet, IL	360	H	Washington, DC	840	Q
Key West, FL	850	I			

dicted. This observation suggests that local meteorological effects not incorporated in the model are contributing to producing gradients. Indeed, all four measurement sites are unusual. The Denver site is on relatively flat ground near the foothills of the Rocky Mountains; the El Paso site is on a mesa approximately 60 m above flat, irrigated land; the New York site is located in a complex metropolis-ocean-land-bay region; and the Long Beach site is subjected to Santa Ana winds.[19] Therefore, the anomaly is attributed to local effects on the probability distributions measured at a single point. If it were possible to measure path-averaged distributions for the four anomalous sites, the model predictions for them might, indeed, show better agreement.

IV. SUMMARY

This work presents a climatological model for arbitrary locations in the United States. It provides refractivity gradient occurrence distributions for positive gradients. The results fill in the gaps among the 17 locations for which measured distributions have been compiled. The significance of this additional detail is that climate variations can be accounted for with much better geographic resolution than had previously been possible, in the specification of microwave antenna heights. A method which uses these results to determine antenna heights has been developed by Vigants and is described in a companion paper.[20]
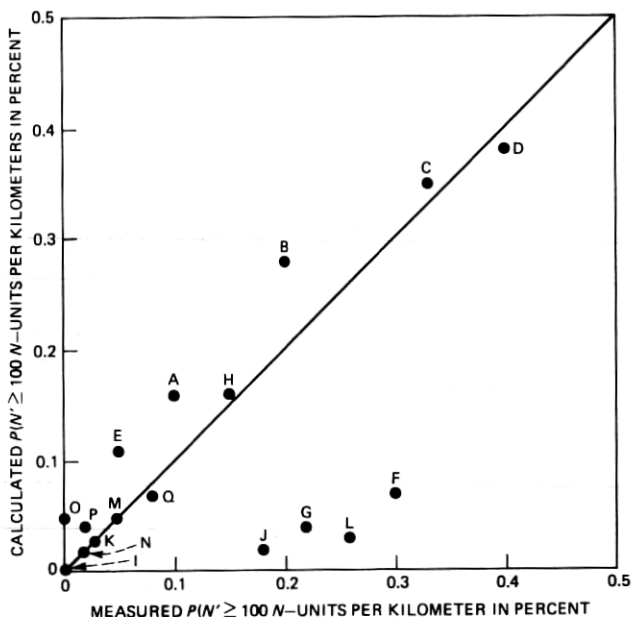
V. ACKNOWLEDGMENTS

Fig. 8—Comparison of model predictions with Samson's measurements for 17 sites.[1] Values plotted are cumulative probabilities for $N' \geq 100$ N-units/km. The line represents perfect agreement between predictions and measurements. Sites are denoted by symbols which are identified in Table III. The four anomalously low points are attributed to the inability of the model to account for unusual local effects.

APPENDIX A

Critical Wind Direction Choice

Climatological information does not exist on the occurrence frequency of wind shifts from continental to maritime directions as air masses traverse the coastlines. However, there is a certain wind direction relative to a coastline which should be related to the occurrence of large-scale moisture advection.

Before air masses reach the coasts, moderately low-level air flow is roughly parallel to the coast with land to the right of the wind vector. Furthermore, this direction is conducive to producing moisture gradients by the mechanism of wind direction variation with height, as discussed in Section 2.1. Therefore, the surface wind direction that most likely causes flow of marine air over continental air adjacent to the coastline is the direction parallel to the coast with land to the right of the wind vector. This is the critical wind direction at the coastline for an ideal linear coastline of infinite extent. In reality, however, the critical direction choice must account for the curvature of the coastline. This is required to ensure that air assumed to be continental (maritime) in origin indeed is underlain by land (water) for a significant

distance upwind from the site. An appropriate choice of minimum distance is the distance travelled by air in one day at an average speed, approximately 300 km.

Because of unavoidable subjectivity required in selecting critical wind directions for some sites, the selection technique is best illustrated with examples. Figure 9 shows nine sites along the southeast U.S. coast, three each along lines drawn perpendicular to the Atlantic Ocean coast from three different coastal sites: A, B, and C. Critical directions for line AA' are parallel to the coast because land lies upwind along this vector for a distance of at least 300 km. This assures that air arriving at sites along line AA' is indeed continental. Such an assurance is not obtained for sites along line BB' if the critical directions are chosen parallel to the coast at B. The directions are chosen so that there is a 300-km air flow trajectory flow over land upwind from sites along BB', as shown in Fig. 9.

The situation at site C is complementary to that at site B. Here, the critical wind direction is chosen so that the wind vector is underlain by water for a distance of 300 km upwind from site C. The critical direction at the other two sites along CC' is chosen assuming that maritime air has its source over the Atlantic Ocean rather than the Gulf of Mexico. This is done since a gulf source would require a critical direction at site C', e.g., as shown by the dotted arrow in Fig. 9. This direction, in turn, would imply continental air originating in the southern half of the Florida peninsula. Obviously, this cannot be considered a source of dry, continental air. Critical direction choices illustrated in the above examples are typical of those made for nearly all locations of the United States.

APPENDIX B

Empirical Determination of a and m_2

The values of a and m_2 for the interior regions are obtained by comparing measured refractivity gradient probability distributions for Columbia, Missouri.[1] The only other interior sites for which measured distributions are available (Denver and El Paso) are characterized by unusual physiographical features (Section III) and are deemed unsuitable for specifying a and m_2. Values are obtained for μ, f_i, V, and m for Columbia. $H = 1$ is used for comparing the model with point gradient measurements (see Section 2.1.1). The value for σ_0 obtained for coastal regions is used. From eq. (9b), σ_{sI} for Columbia is given by $\sigma_{sI} = $ constant $\times a(30 + m_2)$, where the constant is evaluated from the above values.

Determining the optimum agreement between calculated N' distributions (using σ_{sI} as specified above) and the measured N' distribution
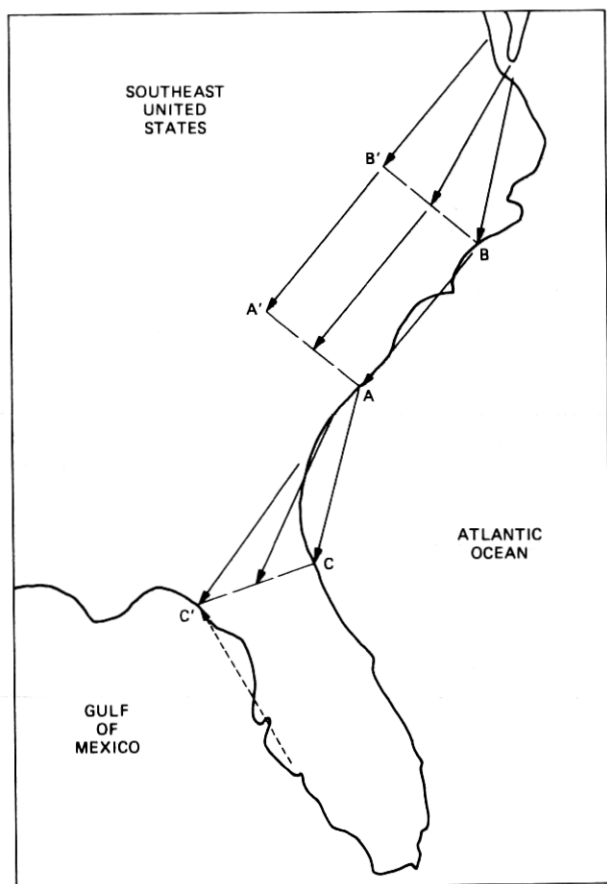
Fig. 9—Examples of critical wind-direction choice. Dashed lines are perpendicular to the Atlantic Coast. Arrows represent critical wind directions chosen for sites at their tips. Arrow length is 300 km (see Appendix A).

for Columbia, yields a relationship between a and m_2. We determine the remaining variable by subjecting calculated values of $\sigma_{sI}(m)$ to constraints for the possible range of m: $-50 \leq m \leq 120$. Columbia's surface moisture index[17] of 30 is intermediate within this range. A second point to completely specify a and m_2 is obtained by assuming that $\sigma_{sI}(m = 120)$ for Columbia is equal to the smallest value of $\sigma_{sC}(m = 120)$ calculated for all of the 14 noninterior sites. Thus, we determine that $a = 4.7 \times 10^{-5}$ and $m_2 = 100$.

REFERENCES

1. C. A. Samson, "Refractivity Gradients in the Northern Hemisphere," Office of Telecommunications Report 75-59, U.S. Dept. of Commerce, April 1975.

2. B. R. Bean, et al., *A World Atlas of Atmospheric Radio Refractivity*, ESSA Monograph 1, Washington, D.C.: U.S. Govt. Printing Office, 1966, pp. 53–8.
3. H. T. Dougherty, "A Survey of Microwave Fading Mechanisms, Remedies, and Applications," ESSA Tech. Rep., ERL 69-WPL 4, 1968.
4. F. Ikegami, et al., "Variation of Radio Refraction in the Lower Atmosphere," IEEE Trans. Antenn. Prop., *AP-16*, No. 2 (March 1968), pp. 194–200.
5. T. Akiyama and O. Sasaki, "Statistical Distribution and Maximum Critical Value for Refractivity Gradient Variation," Rev. Electrical Commun. Lab., *27* (1979), pp. 841–8.
6. A. Vigants, private communication, 1979.
7. B. R. Bean and E. J. Dutton, *Radio Meteorology*, New York: Dover, 1968.
8. H. Moses, W. C. Ashby, and M. A. Bogner, "Dewpoint Temperature Inversions," J. Appl. Meteorol., 7 (April 1968), pp. 206–16.
9. The Analysis and Forecasting of Atmospheric Radar Refractivity, NAVAIR Report 50-1P-1, Naval Weather Service Command, July 1967.
10. R. M. Holmes and J. L. Wright, "Measuring the Effects of Surface Features on the Atmospheric Boundary Layer with Instrumented Aircraft," J. Appl. Meteorol., *17* (August 1978), pp. 1163–70.
11. J. Neumann, "On the Rotation Rate of the Direction of Sea and Land Breezes," J. Atmos. Sci., *34* (1977), pp. 1913–7.
12. K. M. Zishka, "Climatology of Cyclones and Anticyclones Over the North American Continent and Surrounding Ocean Environs for January and July, 1950–1977," M. S. thesis, Purdue University (May 1979).
13. C. R. Hosler, "Low-Level Inversion Frequency in the Contiguous United States," Mon. Weather Rev., *89* (September 1961), pp. 319–39.
14. *The National Atlas of the United States of America*, Washington: U.S. Depart. Interior Geological Survey, 1970, plate 62.
15. *Weather Atlas of the United States*, Detroit: Gale Research, June 1968, pp. 237, 240, 243, 246.
16. *Ibid.*, pp. 4, 19, 34, 49.
17. C. W. Thornthwaite, "An Approach Toward a Rational Classification of Climate," Geogr. Rev., *38* (1948), pp. 55–94.
18. D. C. Livingston, *The Physics of Microwave Propagation*, Englewood Cliffs, New Jersey: Prentice-Hall, 1970.
19. W. T. Sommers, "Strong Mountain Downslope Wind Field Experiment Using Surface Station, Monostatic Acoustic Sounder, and Rawinsonde Observations," *Fourth Symposium on Meteorological Observations and Instrumentation*, Denver, Colorado, April 10–14, 1978, American Meteorological Society: Boston, 1978, pp. 339–44.
20. A. Vigants, "Microwave Radio Obstruction Fading," B.S.T.J., this issue.